www.elsevier.com/locate/jbiomech

Automated Finite Element Modeling of the Lumbar Spine: Using a Statistical Shape Model to Generate a Virtual Population of Models

J.Q. Campbell, A. Petrella

PII: S0021-9290(16)30581-4
DOI: http://dx.doi.org/10.1016/j.jbiomech.2016.05.013
Reference: BM7732

To appear in: *Journal of Biomechanics*

Received date: 31 December 2015
Revised date: 22 March 2016
Accepted date: 15 May 2016

Cite this article as: J.Q. Campbell and A. Petrella, Automated Finite Elemen Modeling of the Lumbar Spine: Using a Statistical Shape Model to Generate Virtual Population of Models, *Journal of Biomechanics* http://dx.doi.org/10.1016/j.jbiomech.2016.05.013

Automated Finite Element Modeling of the Lumbar Spine:

Using a Statistical Shape Model to Generate a Virtual Population of Models

J.Q. Campbell[a,b] and A. Petrella[a]

[a] Department of Mechanical Engineering, Colorado School of Mines, 1500 Illinois St., Golden, Colorado, USA
[b] Vector Scientific Inc., Colorado, USA

Abstract

Population-based modeling of the lumbar spine has the potential to be a powerful clinical tool. However, developing a fully parameterized model of the lumbar spine with accurate geometry has remained a challenge. The current study used automated methods for landmark identification to create a statistical shape model of the lumbar spine. The shape model was evaluated using compactness, generalization ability, and specificity. The primary shape modes were analyzed visually, quantitatively, and biomechanically. The biomechanical analysis was performed by using the statistical shape model with an automated method for finite element model generation to create a fully parameterized finite element model of the lumbar spine. Functional finite element models of the mean shape and the extreme shapes (±3 standard deviations) of all 17 shape modes were created demonstrating the robust nature of the methods. This study represents an advancement in finite element modeling of the lumbar spine and will allow population-based modeling in the future.

1. Introduction

Population-based modeling has been used to meaningful effect in biomechanics by capturing the influence of anatomical variation in many body regions (Bischoff et al., 2014). There are several potential applications of this method in the lumbar spine from evaluating the effects of degeneration on biomechanics to pre-clinical evaluation of devices. However, in the lumbar spine, developing a fully parameterized model with realistic geometry has remained a challenge (Dreischarf et al., 2014). A new method for automated landmark identification in the lumbar spine (Campbell and Petrella, 2015), in concert with statistical shape modeling (SSM), has potential to address this challenge. Creation and evaluation of a SSM of the lumbar spine for use in population-based finite element (FE) modeling was the focus of the current study.

SSM uses principal component analysis (PCA) to determine the primary modes of variation in shape among a training set of specimens (Dryden and Mardia, 1998; Jolliffe, 2002). There are numerous applications of SSM in biomechanics from improving registration in medical imaging applications to creation of FE models (Sarkalkan et al., 2014). Recently, the first SSM of the full lumbar spine was published (Rasoulian et al., 2013), but the primary application of that model was medical imaging segmentation. To our knowledge, no lumbar SSM has been previously reported for use in biomechanical analysis or FE modeling.

SSM has been successfully used with FE modeling and probabilistic methods to study how shape influences results in the knee, tibia, femur, and radius (Bischoff et al., 2014; Laz and Browne, 2010). Single bone SSMs have generally been used to study how shape influences fracture risk (Bryan et al., 2010, 2009; Querol et al., 2006). In the knee, motion and contact forces have been studied in relation to changes in shape and alignment of the different bones (Baldwin et al., 2010; Fitzpatrick et al., 2011; Rao et al., 2013).

In the lumbar spine the influence of geometry on biomechanics has primarily been studied using simplified FE models based on primitive shapes that can be more easily parameterized and modified but do not realistically represent the complex geometry found in real subjects (Meijer et al., 2011; Niemeyer et al., 2012). Particularly in the facet joints, the complex natural shape can be important to biomechanical outcomes (Holzapfel and Stadler, 2006). One of the greatest challenges in creating a parameterized lumbar spine model, with a SSM or other method, is capturing the variation in facet joint shape while maintaining proper facet joint articulation and alignment. Dreischarf et al. (2014) pointed out that "incorporating all the main geometric parameters of the lumbar spine into a statistical approach would require a fully parameterized model. The development of such a model; however, has proven to be notoriously difficult." In addition to realistically representing the complex anatomy, to be used effectively in a population-based simulation framework, such a model must also be robust. That is, parametric variations of the model, especially at the extremes of the shape space, must exhibit articulating facet joints (i.e. no initial penetration) and produce functional FE models. The overall goal of the current study was to develop and evaluate a parametric, automated, and robust FE model of the lumbar spine. A SSM was created and evaluated for use in parameterizing anatomical shape. A fully automated algorithm (Campbell and Petrella, 2015) was then used to construct FE models of virtual specimens instantiated from the SSM, and the relationship between shape modes and biomechanics was investigated for all principal components of shape variation represented in the SSM.

2. Materials and methods

2.1. Statistical Shape Model Creation and Evaluation

The statistical shape model (SSM) was based on a training set of 18 cadaveric specimens of unknown demographics. Segmented CT (computed tomography) scans from multiple sources were obtained in the form of STL files (stereo lithography) for L1-L5 of each subject. Each specimen in the training set was run through a previously published automatic landmark identification algorithm (Campbell and Petrella, 2015). The result was a corresponding set of 6,530 landmarks per specimen (1,306 per vertebra). The highest density of landmarks was on the facet joint surfaces to capture the variation in that critical anatomy.

The landmarks for each specimen were aligned to eliminate variation between specimens due to rigid body translation and rotation (Spoor and Veldpaus, 1980). The vertebrae were left in their scanned alignment to preserve the combinations of facet shape and alignment found in the training set. Principal component analysis (PCA) was performed on the landmark coordinates using standard linear methods based on the covariance matrix (Bischoff et al., 2014; Heimann and Meinzer, 2009; Sarkalkan et al., 2014). PCA produced a set of principal components (PCs) each associated with a different mode of shape variation. The PCs can be used in a linear combination with the mean shape to produce any number of virtual specimens exhibiting normal anatomical variation.

The SSM was evaluated using compactness, generalization ability, and specificity. Common methods for calculating these measures may be found in the literature (Heimann and Meinzer, 2009; Rasoulian et al., 2013; Styner et al., 2003). Compactness describes the number of modes required to represent a given percent of the shape variation. Generalization ability is a measure of the SSM's ability to represent a new specimen that was not part of the training set. Generalization was calculated by performing a leave-one-out analysis. Each specimen in the training set was sequentially left out of the SSM, a new shape model was created with the

remaining specimens, shape modes were added sequentially, and the parameters of the shape model were all optimized to fit the left out specimen. The result was the average error and maximum error, in terms of Euclidian distance, between the corresponding landmarks of the optimized virtual specimen and the left out specimen. Specificity is a measure of the SSM's ability to represent valid specimens. Shape modes were included in the SSM incrementally and 200 virtual specimens were randomly generated for each set of shape modes using ±3 standard deviations of the PCs included. Virtual specimens were compared to the closest specimen in the training set in terms of minimum average Euclidian distance error.

2.2. Shape Analysis

A SSM model produces a set of orthogonal shape modes that describe the variation in the shape space of the training set. All shape modes of the SSM of the lumbar spine were analyzed qualitatively, quantitatively, and biomechanically. For brevity, results from only the first five shape modes are reported here. SSMs are often analyzed qualitatively based on visual inspection of the models they produce (Bischoff et al., 2014; Fitzpatrick et al., 2011; Peloquin et al., 2014; Rao et al., 2013; Sarkalkan et al., 2014). The first five shape modes were plotted using ±3 standard deviations of the PCs and evaluated visually.

A quantitative analysis of the shape modes was also performed to verify the visual assessments and analyze anatomical variation that was not obvious on inspection. The quantitative analysis was accomplished by taking direct anatomical measurements of the mean shape and models produced using ±3 standard deviations of each of the PCs. Since many of the landmarks used in the present study to create the shape model had specific anatomical meaning, measurements were easily made on each virtual specimen. Due to the large number of

measurements generated, only a subset of relevant measures was reported based on average variations, over all five vertebrae (four FSUs) in each virtual specimen.

In order to analyze the influence of each shape mode on variation in the anatomical measurements, a percent contribution parameter was calculated as follows:

$$\mathrm{Range_n} = \mathrm{Abs}(\mathrm{Measure_{n+}} - \mathrm{Measure_{n-}}) \quad (1)$$

$$\%\mathrm{Contrib_n} = \frac{\mathrm{Range_n}}{\sum_{i=1}^{N} \mathrm{Range_i}} \quad (2)$$

where n is the number of the mode of interest; Measure is the anatomical measurement or other output variable associated with the ±3 standard-deviation extreme shape of that mode; $\mathrm{Range_n}$ represents the total range of the Measure for mode n; and N = 17 is the total number of modes calculated.

Biomechanical analysis of the SSM was conducted by running FE simulations with auto-generated models based on the mean virtual specimen and each of the 17 shape modes using ±3 standard deviations of the PCs. A total of 35 FE models (L1-L5) were created using the SSM in conjunction with the previously published automated FE generation method (Campbell and Petrella, 2015). The details of the FE model including mesh convergence, direct validation for a single specimen, and indirect validation for the 18 subjects used in the SSM training set are described in a separate publication (Campbell et al., 2016). One generalized set of material properties was used for all of the simulations to isolate the influence of anatomical variation (Table 1). All of the simulations were run in Abaqus Standard v6.14-5 (Simulia, Johnston, RI, USA). For each virtual specimen modeled, a 7.5 N m pure bending moment was applied in

directions of flexion, extension, left and right lateral bending, and left and right axial rotation. For each of the 210 simulations, values of rotation, disc pressure, and facet force were recorded. In order to analyze the contributions of each shape mode to the biomechanical output, the $\%Contrib_n$ given by (2) was calculated.

3. Results

3.1. SSM Evaluation

The SSM was evaluated using measures of compactness, generalization ability, and specificity. Figure 1 shows the results for compactness. The first shape mode accounted for nearly 60% of the shape variation in the lumbar spine. Eight modes were required for the SSM to capture over 90% of the shape variation and 12 modes were necessary to capture over 95% of the variation. For generalization ability the average Euclidian distance error decreased from 3.65 mm (±0.63) with one shape mode to 2.78 mm (±0.45) with 16 modes. The maximum error decreased from 13.9 mm (±2.7) with one mode to 13.1 mm (±2.0) with 16 modes. The specificity measure was calculated by evaluating how close specimens from the training set were to virtual specimens. The average error increased as the virtual specimens got more complex due to addition of higher-order shape modes. The average error with 1 mode was 3.11 mm (±0.47) and the average error with 17 modes was 3.76 mm (±0.64).

3.2. Shape Analysis

Analysis of lumbar spine shape variation was performed with qualitative visual assessment, quantitative analysis, and biomechanical analysis. Figure 2 illustrates the first five modes of shape variation in the SSM. Mode 1 appears to be a scaling mode with effect on lordosis, disc height, and the angle of the transverse processes in the frontal plane. Mode 2 appears to

primarily affect lordosis and disc height without scaling. Mode 3 appears to primarily influence the depth of the vertebral bodies. Mode 4 appears to affect the length and width of the vertebrae with minimal effect on height. Mode 5 appears to mainly influence the posterior spinous process height and transverse process width.

The quantitative analysis of shape variation was performed by comparing the shape modes to average anatomical measurements on the virtual specimens. The quantitative measurements provide details about the changes in shape that are not easily visualized. Table 2 provides anatomical measurements for the mean shape and the percent contribution of each shape mode to each measurement. The results show that Mode 1 has the largest percent contribution to 9 of the 21 anatomical measures evaluated. The quantitative analysis confirmed that Mode 1 contributed most to scaling, disc height, lordosis, and transverse process frontal plane angle (as shown in Figure 2). Mode 2 contributed primarily to lordosis and disc height, only slightly less than Mode 1. Mode 3 controlled variation in end-plate depth without change in end-plate height (again, visible in Figure 2), and it also exhibited a similar contribution to end-plate width. Mode 3 contributed the greatest to variation in inferior facet curvature. Mode 4 was the largest contributor to spinous process length and canal depth. Mode 4 was also the largest contributor to superior and inferior facet card Ax angle, which could not be easily appreciated in Figure 2. Mode 5 was the largest contributor to spinous process posterior height. The maximum contributions to multiple measurements were made by modes higher than the five shown in Table 2 – Modes 6, 11, and 12 had the largest contributions to three of the four facet curvature metrics.

The biomechanical analysis of the SSM was conducted by running FE simulations with a model auto-generated from the mean shape of the SSM and models based on extreme variations

(±3 standard deviations) in each of the 17 shape modes. All 35 FE models based on the SSM exhibited articulating facet contact surfaces with no initial penetration. Figure 4 illustrates the results for rotation, disc pressure, and facet force for the first five shape modes. The results demonstrate that, in most cases, all of the first five shape modes have some effect on lumbar biomechanics. Although, in many cases the shape modes do not have an equal effect in both directions from the mean. In fact, for axial rotation the facet forces almost all decrease relative to the mean shape. The different shape modes generally had different effects with each bending direction for rotation and facet force. However, the effect of each shape mode on disc pressure was fairly consistent in each of the bending directions.

The effect of each shape mode on the biomechanics of the lumbar spine can be evaluated by examining the percent contributions shown in Table 3. The results show that Mode 4 contributed the most to the variation in biomechanics for 3 of the 8 output metrics. Modes 1 through 4 contributed a similar amount to extension rotation. Modes 2, 4, and 5 all contributed to flexion rotation. Mode 1 contributed the most to rotation and facet forces in axial rotation. Modes 2 and 4 contributed the greatest amount to rotation and facet forces in lateral bending. Mode 4 contributed the most to disc pressure over all bending directions. Mode 14 contributed the most to facet forces in extension.

4. Discussion

The current study successfully demonstrated the use of a SSM combined with automated methods for landmark identification and FE model generation to create a fully parameterized FE model of the lumbar spine. Functional FE models of the mean shape and the extreme shapes (±3 standard deviations) of all 17 shape modes were created. While all 17 shape modes would likely not be included in practical use of the shape model, this study demonstrates that the methods are

robust even at the boundaries of the shape space (±3 standard deviations) for all 17 modes. This study represents an advancement in FE modeling of the lumbar spine and will empower population-based modeling in future work.

The lumbar spine SSM was evaluated for compactness, generalization ability, and specificity. The first eight shape modes accounted for over 90% of the shape variation which is in the range of other models of the knee and spine (Baldwin et al., 2010; Peloquin et al., 2014; Rao et al., 2013; Rasoulian et al., 2013). Rasoulian et al. (2013) reported compactness, generalization, and specificity for a lumbar shape model. However, they separated modes of shape and pose variation in their model while these parameters were combined in the current study. Therefore, direct comparison of our results to theirs may not be appropriate.

The difference in strategy for addressing pose between the current study and the SSM of Rasoulian et al. is an important topic in SSM (Bischoff et al., 2014). When a shape model is intended to represent the shape of multiple structures as well as their relative positions, shape and pose can be handled together or separately. The choice may depend on the application of the SSM. In medical imaging and segmentation it has been recommended that shape and pose be treated separately (Gorczowski et al., 2010; Rasoulian et al., 2013). The application in Gorczowski et al. (2010) was to study autism by analyzing various structures in the brain, in which case it may also be more useful to analyze shape and pose separately. In the lumbar spine Rasoulian et al. (2013) argued that shape and pose should be handled separately because they are "not necessarily correlated." Again, Rasoulian et al. (2013) were using an SSM for medical imaging where it is important that the SSM be capable of identifying the same structure in multiple poses. In the current study we have used FE models to study lumbar spine biomechanics. In this application it is most important to create virtual specimens with correctly

articulating joints. There are eight facet joints in the L1-L5 lumbar spine, and the shapes of the facet contact surfaces are biomechanically coupled with the poses of the vertebrae. Therefore, in the current study, we chose to treat shape and pose together in the SSM. This method is consistent with many SSMs of the knee where joint contact surfaces are also an important issue (Baldwin et al., 2010; Bredbenner et al., 2010; Fitzpatrick et al., 2011; Rao et al., 2013). The high level of robustness of the FE models in the current study support the strategy of treating shape and pose together for the application of FE modeling in the lumbar spine.

The shape modes in the current SSM were analyzed in terms of the biomechanics produced by varying each of the shape modes. The results showed that several of the shape modes contributed to similar changes in biomechanical outcomes. Mode 4, which only accounted for 6% of the total shape variation, was shown to have the greatest influence on 3 of the 8 biomechanical metrics studied. One higher mode (14) was found to have a large influence on a specific biomechanical parameter, facet force in extension. This highlights the fact that shape modes representing a relatively small percent of the total variation in lumbar spine geometry could have a large effect on biomechanics. But higher modes may also be affected by noise introduced through the imaging and segmentation process. Researchers may want to consider this phenomenon when determining how many shape modes to keep in a SSM model.

Prior studies used FE models to examine how changes in lumbar spine anatomy influenced biomechanics (Meijer et al., 2011; Niemeyer et al., 2012). While the current study evaluated how shape modes influenced anatomy and biomechanics, the current study was not explicitly designed to investigate how variations in isolated anatomical measurements influence biomechanics. The SSM intentionally combines variation in anatomical measurements into a small number of distinct shape modes. Using the SSM in a larger population-based probabilistic

study, similar to the study design of Niemeyer et al. (2012), would be the appropriate way to analyze how individual anatomical measures influence biomechanics.

While the current automated modeling method was designed to be used for population-based FE modeling, there are limitations. The linear PCA methods used in this study have known limitations for accurately capturing shape variations that are strongly driven by bending or rotation (e.g., lumbar lordosis). Ali et al. (2012) found a linear 2D shape model of the lumbar spine produced unrealistic geometry when the first mode was varied to three standard deviations above the mean. In the present study we did not see geometry distortion at the boundaries of the shape space (±3 standard deviations), either through visual inspection or a loss of FE solution stability – the latter condition being strongly influenced by mesh distortion and non-conformal facet contact associated with distorted geometry. Based on these observations, we believe that the linear PCA methods provided acceptable results in the present study. However, non-linear methods are available (Heap and Hogg, 1996; Heimann et al., 2009; Rasoulian et al., 2013; Sarkalkan et al., 2014) and may be more appropriate for generating not only realistic virtual lumbar shapes, but, perhaps more importantly, realistic biomechanics from FE models generated by SSM. Evaluations of this issue by comparing linear and non-linear PCA methods should be addressed in future work.

The evaluation of the SSM generalization ability showed that the current model does not capture some aspects of shape variation in the population and a larger training set would likely help improve that. The current methods are also specific to the FE modeling techniques used. The current FE model uses rigid vertebrae and endplates, which are reasonable for the loading scenarios studied (Campbell and Petrella, 2015; Campbell et al., 2016), but are not appropriate for all applications. There are also potential improvements to treatment of the intervertebral disc

geometry that may be important for consideration of clinical conditions including substantial degeneration. For example, the current model captures variation in disc height and angle, but does not capture the true shape of the annulus and nucleus or their relative volumetric proportions. A recent study reported a SSM of the L3-L4 disc, but it does not capture the shape of the nucleus (Peloquin et al., 2014). The current modeling method also uses the bone surfaces of the facets to represent the anatomical shape of the facet cartilage surfaces and their respective gaps, but the cartilage thickness is based on generalized measurements (Campbell and Petrella, 2015; Woldtvedt et al., 2011). A linked CT and MRI dataset could potentially be used to address those limitations. Finally, the current method uses the as-scanned alignment of the specimens for the SSM and FE models. Our training set of scans came from multiple sources, and consistent neutral alignment of all specimens could not be ensured. While the results of a related validation study suggest that the as-scanned alignment produced reasonable biomechanical results (Campbell et al., 2016), a training set of consistently aligned specimens scanned in consistent neutral alignment would improve the SSM (Rao et al., 2013).

Future work will focus on expanding the current training set and applying the SSM to population-based FE modeling of spine biomechanics. Although anatomical variation captured by the SSM is a central element of a population-based model, material property variation is another critical factor that remains a challenge. However, established probabilistic methods (Easley, 2007; Laz and Browne, 2010) allow material properties to be defined by appropriate probability distributions that can be inferred from the literature, and systematic material changes could be used to tailor a model to specific subpopulations (severe disc degeneration, for example). Other applications of a probabilistic modeling strategy include pre-clinical evaluation of new devices, planning and evaluation of surgical procedures, and analysis of the

biomechanical impact of anatomical variations. The methods presented here facilitate the use of probabilistic FE tools to study these important lumbar spine topics in the future.

Conflict of Interest Statement

We have no conflict of interest to declare.

Acknowledgement

This work was supported in part by the U.S. National Science Foundation under Grant 846845.

References

Ahmed, A.M., Duncan, N.A., Burke, D.L., 1990. The effect of facet geometry on the axial torque-rotation response of lumbar motion segments. Spine (Phila. Pa. 1976). 15, 391-401.

Ali, A., Cowan, A.-B., Gregory, J., Aspden, R., Meakin, J., 2012. The accuracy of active shape modelling and end-plate measurements for characterising the shape of the lumbar spine in the sagittal plane. Comput. Methods Biomech. Biomed. Engin. 15, 167-172.

Baldwin, M.A., Langenderfer, J.E., Rullkoetter, P.J., Laz, P.J., 2010. Development of subject-specific and statistical shape models of the knee using an efficient segmentation and mesh-morphing approach. Comput. Methods Programs Biomed. 97, 232–240.

Bischoff, J.E., Dai, Y., Goodlett, C., Davis, B., Bandi, M., 2014. Incorporating Population-Level Variability in Orthopedic Biomechanical Analysis: A Review. J. Biomech. Eng. 136, 021004.

Bredbenner, T.L., Eliason, T.D., Potter, R.S., Mason, R.L., Havill, L.M., Nicolella, D.P., 2010. Statistical shape modeling describes variation in tibia and femur surface geometry between Control and Incidence groups from the Osteoarthritis Initiative database. J. Biomech. 43, 1780–1786.

Bryan, R., Mohan, P.S., Hopkins, A., Galloway, F., Taylor, M., Nair, P.B., 2010. Statistical modelling of the whole human femur incorporating geometric and material properties. Med. Eng. Phys. 32, 57–65.

Bryan, R., Nair, P.B., Taylor, M., 2009. Use of a statistical model of the whole femur in a large scale, multi-model study of femoral neck fracture risk. J. Biomech. 42, 2171–2176.

Campbell, J.Q., Petrella, A.J., 2015. An Automated Method for Landmark Identification and Finite Element Modeling of the Lumbar Spine. IEEE Trans. Biomed. Eng. 62, 2709 – 2716.

Campbell, J.Q., Coombs, D., Rao, M., Rullkoetter, P., Petrella A, 2016. Automated Finite Element Modeling of the Lumbar Spine: Verification and Validation with 18 Specimen-Specific Models. Submitted to the J. Biomech December 30, 2015 and attached as supplementary material to the current submission.

Di Angelo, L., Di Stefano, P., 2015. A new method for the automatic identification of the dimensional features of vertebrae. Comput. Methods Programs Biomed. 121, 36–48.

Dreischarf, M., Zander, T., Shirazi-Adl, A., Puttlitz, C.M., Adam, C.J., Chen, C.S., Goel, V.K., Kiapour, A., Kim, Y.H., Labus, K.M., Little, J.P., Park, W.M., Wang, Y.H., Wilke, H.J., Rohlmann, A., Schmidt, H., 2014. Comparison of eight published static finite element models of the intact lumbar spine: Predictive power of models improves when combined together. J. Biomech. 47, 1757–1766.

Dryden, I., Mardia, K., 1998. Statistical shape analysis. Wiley, Chichester.

Easley, S.K., Pal, S., Tomaszewski, P.R., Petrella, A.J., Rullkoetter, P.J., 2007. Finite element-based probabilistic analysis tool for orthopaedic applications. Comput. Methods Prog. Biomed. 85, 32-40.

Fitzpatrick, C.K., Baldwin, M.A., Laz, P.J., FitzPatrick, D.P., L. Lerner, A., Rullkoetter, P.J., 2011. Development of a statistical shape model of the patellofemoral joint for investigating relationships between shape and function. J. Biomech. 44, 2446–2452.

Gorczowski, K., Styner, M., Jeong, J.Y., Marron, J.S., Piven, J., Hazlett, H.C., Pizer, S.M., Gerig, G., 2010. Multi-object analysis of volume, pose, and shape using statistical discrimination. Pattern Anal. Mach. Intell. IEEE Trans. 32, 652–661.

Heap, T., Hogg, D., 1996. Extending the point distribution model using polar coordinates. Image and Vision Computing 14, 589-599.

Heimann, T., Meinzer, H.P., 2009. Statistical shape models for 3D medical image segmentation: A review. Med. Image Anal. 13, 543–563.

Holzapfel, G.A., Stadler, M., 2006. Role of facet curvature for accurate vertebral facet load analysis. Eur. Spine J. 15, 849–856.

Jolliffe, I.T., 2002. Principal Component Analysis, Second Edition. John Wiley & Sons, Ltd.

Lavaste, F., Skalli, W., Robin, S., Roy-Camille, R., Mazel, C., 1992. Three-dimensional geometrical and mechanical modelling of the lumbar spine. J. Biomech. 25, 1153–1164.

Laz, P.J., Browne, M., 2010. A review of probabilistic analysis in orthopaedic biomechanics. Proc. Inst. Mech. Eng. H. 224, 927–943.

Meijer, G.J.M., Homminga, J., Veldhuizen, A.G., Verkerke, G.J., 2011. Influence of interpersonal geometrical variation on spinal motion segment stiffness: implications for patient-specific modeling. Spine (Phila. Pa. 1976). 36, E929–E935.

Niemeyer, F., Wilke, H.J., Schmidt, H., 2012. Geometry strongly influences the response of numerical models of the lumbar spine-A probabilistic finite element analysis. J. Biomech. 45, 1414–1423.

Panjabi, M., Goel, V., Oxland, T., Takata, K., Duranceau, J., Krag, M., Price, M., 1992. Human lumbar vertebrae: quantitative three-dimensional anatomy. Spine (Phila. Pa. 1976). 17, 299–306.

Panjabi, M., Oxland, T., Takata, K., Goel, V., Duranceau, J., Krag, M., 1993. Articular facets of the human spine. Quantitative three-dimensional anatomy. Spine (Phila. Pa. 1976). 18, 1298–1310.

Peloquin, J.M., Yoder, J.H., Jacobs, N.T., Moon, S.M., Wright, A.C., Vresilovic, E.J., Elliott, D.M., 2014. Human L3L4 intervertebral disc mean 3D shape, modes of variation, and their relationship to degeneration. J. Biomech. 47, 2452–2459.

Querol, L.B., Büchler, P., Rueckert, D., Nolte, L.P., Ballester, M.Á.G., 2006. Statistical finite element model for bone shape and biomechanical properties. Med. Image Comput. Comput. Interv. 405–411.

Rao, C., Fitzpatrick, C.K., Rullkoetter, P.J., Maletsky, L.P., Kim, R.H., Laz, P.J., 2013. A statistical finite element model of the knee accounting for shape and alignment variability. Med. Eng. Phys. 35, 1450–1456.

Rasoulian, A., Rohling, R., Abolmaesumi, P., 2013. Lumbar spine segmentation using a statistical multi-vertebrae anatomical shape+pose model. IEEE Trans. Med. Imaging 32, 1890–1900.

Sarkalkan, N., Weinans, H., Zadpoor, A.A., 2014. Statistical shape and appearance models of bones. Bone 60, 129–140.

Semaan, I., Skalli, W., Veron, S., Templier, A., Lassau, J.P., Lavaste., F., 2001. Anatomie quantitative tridimensionnelle du rachis lombaire. Rev. Chir. Orthop. Reparatrice Appar. Mot. 83, 340–353.

Spoor, C., Veldpaus, F., 1980. Rigid body motion calculated from spatial co-ordinates of markers. J. Biomech.

Styner, M.A., Rajamani, K.T., Nolte, L.-P., Zsemlye, G., Székely, G., Taylor, C.J., Davies, R.H., 2003. Evaluation of 3D correspondence methods for model building. Inf. Process. Med. Imaging 18, 63–75.

Tan, S., Teo, E., Chua, H., 2002. Quantitative three-dimensional anatomy of lumbar vertebrae in Singaporean Asians. Eur. Spine J. 11, 152–158.

Tan, S.H., Teo, E.C., Chua, H.C., 2004. Quantitative three-dimensional anatomy of cervical, thoracic and lumbar vertebrae of Chinese Singaporeans. Eur. Spine J. 13, 137–146.

Woldtvedt, D.J., Womack, W., Gadomski, B.C., Schuldt, D., Puttlitz, C.M., 2011. Finite element lumbar spine facet contact parameter predictions are affected by the cartilage thickness distribution and initial joint gap size. J. Biomech. Eng. 133, 061009.

Wu, G., Siegler, S., Allard, P., Kirtley, C., Leardini, A., Rosenbaum, D., Whittle, M., D'Lima, D.D., Cristofolini, L., Witte, H., Schmid, O., Stokes, I., 2002. ISB recommendation on definitions of joint coordinate system of various joints for the reporting of human joint motion--part I: ankle, hip, and spine. International Society of Biomechanics. J. Biomech. 35, 543–548.

Xu, R., Burgar, A., Ebraheim, N., Yeasting, R., 1999. The quantitative anatomy of the laminas of the spine. Spine (Phila. Pa. 1976). 24, 107-113.

Table 1
Generalized material properties used in the simulations (Campbell et al., 2016).

Fig 1. Plot of the compactness of the SSM by showing cumulative shape variance as shape modes are added to the SSM. Over 90% of the total variance is captured with 8 modes.

Fig 2. Appearance of the first five shape modes from the lumbar spine SSM in both a lateral view and posterior view.

Table 2
Mean shape measurement values and percent contributions of each shape mode to various anatomical measurements (calculations use all 17 modes but only results from modes 1-5 are shown). Values are shaded darkest (maximum) to lightest (zero) for each row. Measures were

averaged over all bones L1-L5. The Max Mode is the shape mode with the maximum % contribution from all modes. The sum of all 17 contributions add up to 100%. Bone volume was estimated by multiplying the total length, width, and height of each vertebra with respect to the recommended ISB coordinate system (Wu et al., 2002). End-plate depth, width, and height were averages of the superior and inferior measurements described by Panjabi et al. (1992). Canal depth and transverse process width were also calculated similar to Panjabi et al. (1992). Transverse process angles in the transverse and frontal planes were calculated similar to Semaan et al. (2001). Spinous process length and spinous process angle were calculated as described in Di Angelo and Di Stefano (2015). The spinous process posterior height was calculated using the distance between landmarks for the most posterior superior point and most posterior inferior point on the spinous process (Campbell and Petrella, 2015). The facet curvatures were measured using two techniques: facet depth from Ahmed et al. (1990) and facet radius from Semaan et al. (2001). The facet card angles Ax and Ay were calculated based on the techniques described by Panjabi et al. (1993).

Fig 3. Results of the biomechanical shape analysis based on FE simulations of the mean shape and models based on the first five shape modes. Simulations were performed in all six primary bending directions. Results are presented for rotation (top), disc pressure (middle), and facet force (bottom), averaged over all levels L1-L5.

Table 3

Percent contributions of each shape mode to biomechanical outputs based on FE model simulations (calculations use all 17 modes but only results from modes 1-5 are shown). Values are shaded darkest (maximum) to lightest (zero) for each row. FE outputs are shown for rotation, disc pressure (averaged over all six bending directions), and facet force (corresponding right and left facet forces averaged). The Max Mode is the shape mode with the maximum % contribution of all modes. The sum of all 17 contributions add up to 100%.

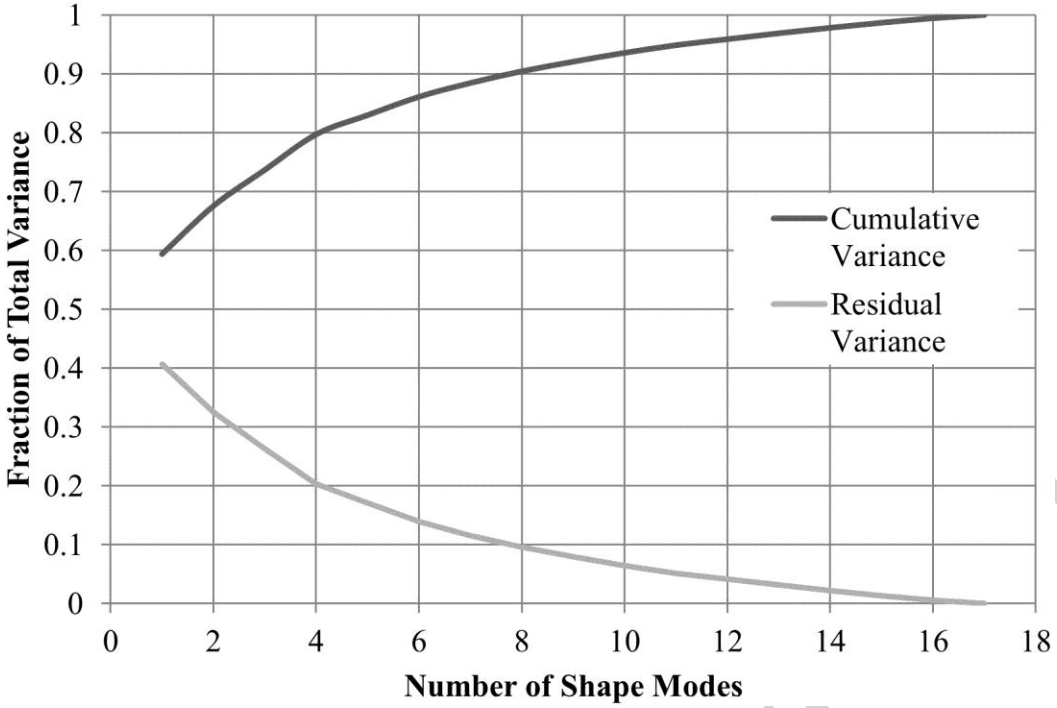

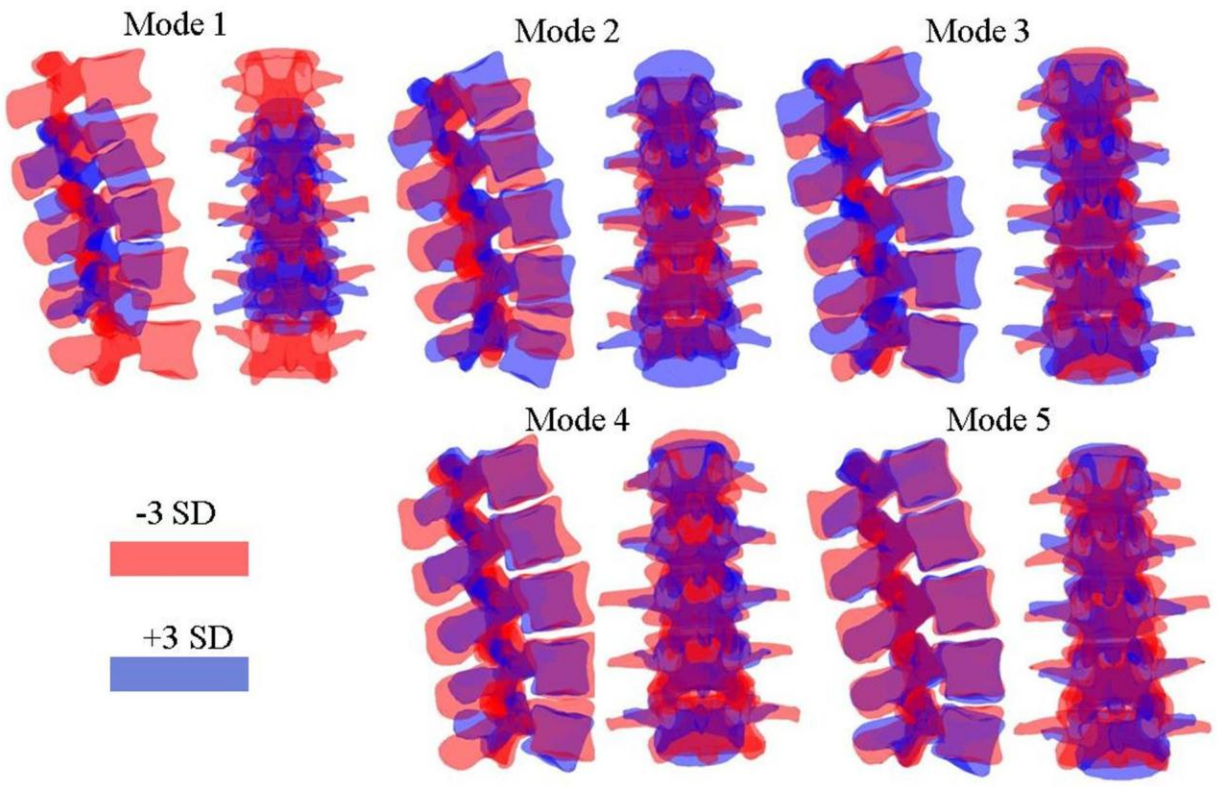

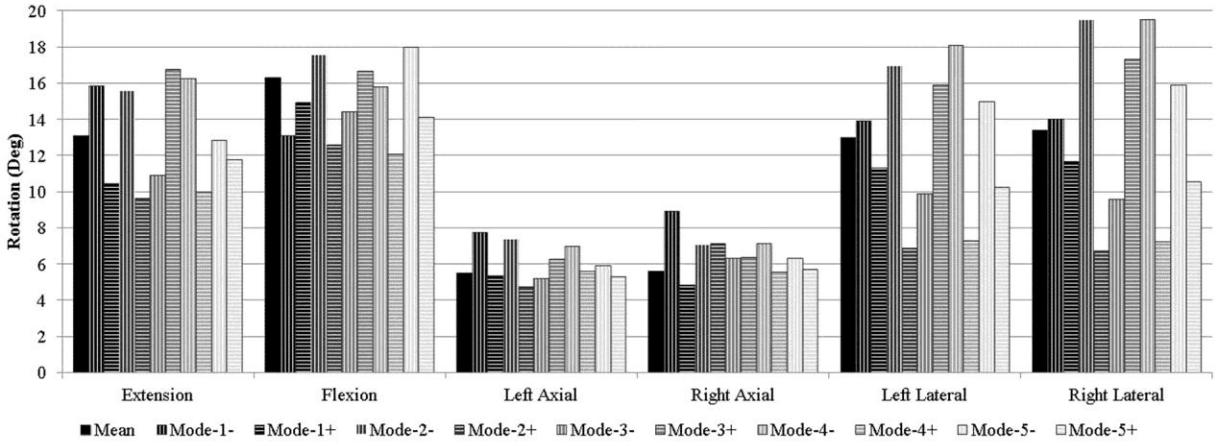

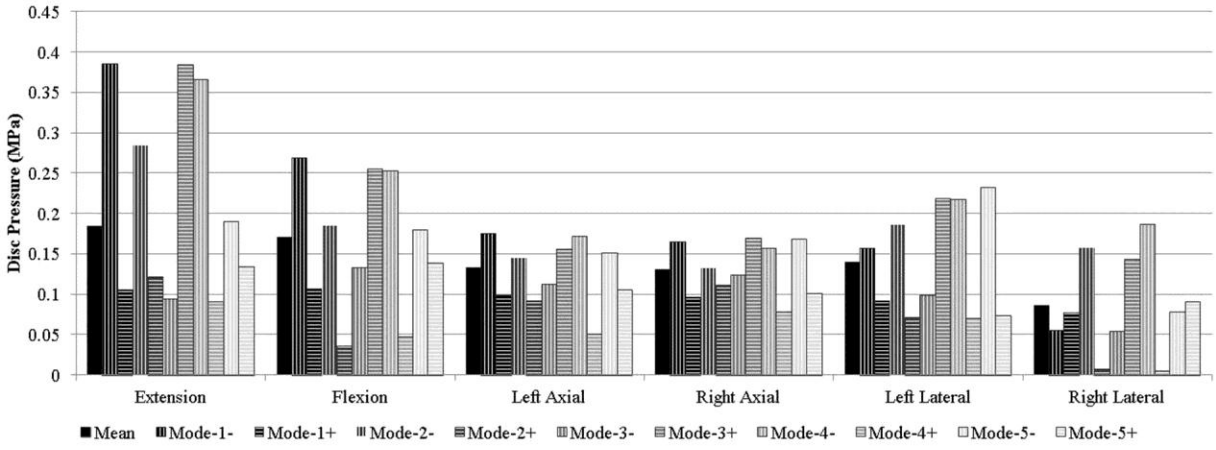

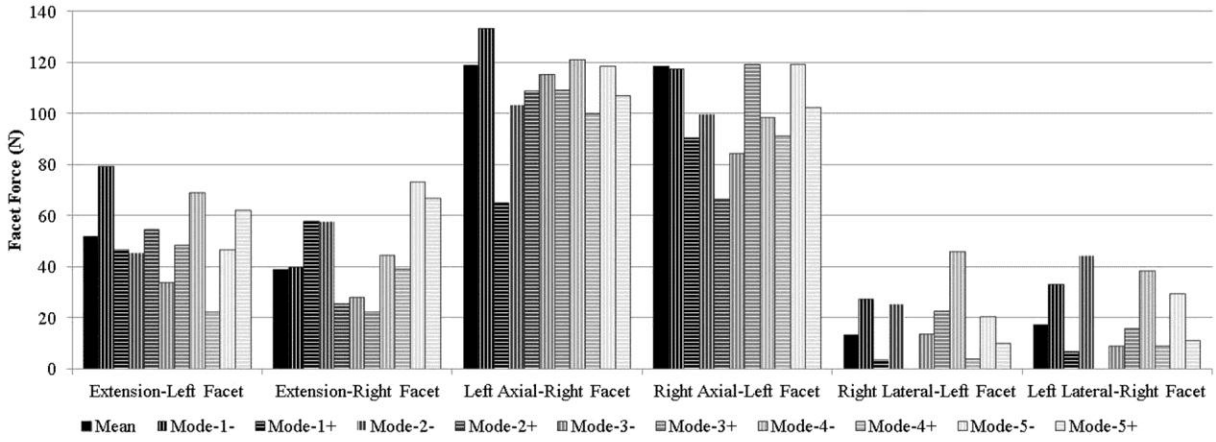

<table>
<tr><td>Bones / Endplates</td><td colspan="6">Rigid</td></tr>
<tr><td>Ligaments</td><td colspan="6">Tension Only, Exponential Force-Displacement</td></tr>
<tr><td rowspan="5">Annulus Fibrosis (Holzapfel-Ogden-Gasser Model)</td><td colspan="2">Matrix</td><td>Fibers</td><td>Anterior</td><td>Lateral</td><td>Posterior</td></tr>
<tr><td rowspan="2">C10 (MPa)</td><td rowspan="2">0.25</td><td>k1 (MPa)</td><td>2</td><td>3</td><td>5</td></tr>
<tr><td>k2</td><td>190</td><td>45</td><td>10</td></tr>
<tr><td rowspan="2">D (1/MPa)</td><td rowspan="2">0</td><td>Angle (deg)</td><td>26</td><td>34.9</td><td>43</td></tr>
<tr><td>Kappa</td><td>0</td><td>0</td><td>0</td></tr>
<tr><td>Nucleus Pulposus</td><td colspan="6">Fluid-Cavity K=2200 MPa</td></tr>
<tr><td>Facet Cartilage</td><td colspan="6">Frictionless, Softened Contact, Linear Pressure-Overclosure, k=100 MPa/mm</td></tr>
</table>

Measurement	Units	Mean	Max Mode	Mode 1	Mode 2	Mode 3	Mode 4	Mode 5
Bone Volume	(mm^3)	273948	1	21%	3%	8%	12%	10%
End-Plate Depth	(mm)	34.3	1	24%	2%	10%	6%	6%
End-Plate Width	(mm)	48.8	1	19%	5%	8%	11%	10%
End-Plate Height	(mm)	27.3	1	27%	10%	2%	10%	9%
Canal Depth	(mm)	20.8	4	3%	9%	8%	13%	11%
Transverse Process Width	(mm)	84.4	6	7%	6%	2%	11%	12%
Spinous Process Length	(mm)	36.2	4	14%	9%	6%	26%	0%
Spinous Process Posterior Height	(mm)	15.8	5	11%	2%	2%	11%	14%
Superior Facet Depth	(mm)	3.4	6	3%	4%	3%	3%	3%
Inferior Facet Depth	(mm)	1.60	12	7%	10%	12%	13%	4%
Superior Facet Radius	(mm)	17.8	11	1%	1%	0%	2%	2%
Inferior Facet Radius	(mm)	17.8	3	7%	10%	26%	5%	0%
Disc Height	(mm)	9.7	1	18%	16%	1%	6%	7%
Lordosis L1-L5	(deg)	24.0	1	20%	20%	2%	7%	5%
Transverse Process Angle Transverse Plane	(deg)	18.9	1	9%	1%	6%	6%	1%
Transverse Process Angle Frontal Plane	(deg)	-0.6	1	23%	11%	10%	2%	3%
Spinous Process Angle	(deg)	-26.7	7	6%	20%	9%	3%	2%
Superior Facet Card Angle Ax	(deg)	-84.8	4	3%	0%	11%	20%	15%
Inferior Facet Card Angle Ax	(deg)	-83.0	4	4%	4%	10%	13%	12%
Superior Facet Card Angle Ay	(deg)	52.1	1	20%	13%	13%	16%	3%
Inferior Facet Card Angle Ay	(deg)	48.2	1	21%	11%	13%	3%	2%

Output Variable	Bending Direction	Max Mode	Mode 1	Mode 2	Mode 3	Mode 4	Mode 5
Rotation	Extension	4	12%	13%	13%	14%	2%
Rotation	Flexion	2	5%	13%	6%	9%	10%
Rotation	Axial	1	17%	7%	3%	8%	3%
Rotation	Lateral	4	4%	17%	10%	17%	7%
Disc Pressure	Average of All	4	13%	13%	14%	20%	7%
Facet Force	Extension	14	2%	3%	1%	6%	1%
Facet Force	Axial	1	21%	6%	6%	7%	6%
Facet Force	Lateral	2	14%	20%	3%	18%	8%